

## Atomic structure and charge transfer in liquid Rb-Te mixtures: An *ab initio* molecular-dynamics simulation

Fuyuki Shimojo and Kozo Hoshino

*Faculty of Integrated Arts and Sciences, Hiroshima University, Higashi-Hiroshima 739-8521, Japan*

Y. Zempo

*Sumitomo Chemical, 6 Kitahara, Tsukuba 300-3294, Japan*

(Received 7 July 1998)

The structural and electronic properties of liquid  $\text{Rb}_x\text{Te}_{1-x}$  mixtures ( $x=0.0, 0.2,$  and  $0.5$ ) are studied by an *ab initio* molecular-dynamics simulation. It is shown that the transition from metallic to semiconducting states by adding Rb atoms is successfully reproduced as an appearance of a dip at the Fermi level of the calculated electronic density of states, and that this transition is closely related to the structural change in the Te chain. For  $x=0.2$ , since the interchain interactions are suppressed by  $\text{Rb}^+$  ions, the Te chains are relatively stabilized in comparison with the pure liquid Te ( $x=0.0$ ). For  $x=0.5$ , more than 50% of Te atoms form  $\text{Te}_2^{2-}$  dimers, which are mixed with short Te chains and  $\text{Rb}^+$  ions. It is also shown by calculating the partial density of states that almost complete charge transfer from Rb to Te occurs in the mixtures. The spatial distribution of the transferred charge in the Te chains is obtained and its correlation to the positions of  $\text{Rb}^+$  ions is investigated. [S0163-1829(99)05405-3]

### I. INTRODUCTION

The solid Te is a typical semiconductor, which has the trigonal structure consisting of infinite twofold-coordinated helical chains of covalently bonded atoms. On the other hand, it is known that the liquid Te exhibits metallic properties such as an electrical conductivity of about  $2000 (\Omega \text{ cm})^{-1}$  near the melting point. As for the structure of liquid Te, the diffraction measurements<sup>1-3</sup> have shown that there is no well-defined first coordination shell in the pair distribution functions which suggests that there exist a high density of threefold-coordinated defects in the liquid phase. This feature is different from the other element in the same element group of chalcogen such as Se; it shows semiconducting properties and it has a clear chain structure in both solid and liquid phases.

To understand such peculiar electronic and atomic structures of liquid Te, several experimental studies have been done for liquid alkali-Te mixtures<sup>4-7</sup> as well as for pure liquid Te. When alkali elements are added into liquid Te, its electrical conductivity decreases monotonically with increasing alkali concentration and the conductivity vs concentration relation does not depend on alkali species;<sup>7</sup> at 50% of alkali concentration, the electrical conductivity is only about  $1 (\Omega \text{ cm})^{-1}$  and its temperature dependence is an activation type. Thus the liquid alkali-Te mixtures show the metal-semiconductor transition by adding alkali elements. It is useful for understanding the cohesive properties of liquid Te to clarify the relation between the electronic properties and the chain structure of Te in liquid semiconducting mixtures.

Fortner *et al.*<sup>5</sup> investigated the structure of liquid K-Te mixture by the neutron diffraction and concluded that nearly complete charge transfer from K to Te occurs, and that the short chains are stabilized as  $\text{Te}_n^{2-}$  ions, so-called ‘‘Zintl ion.’’ They suggested that the K ions terminate these charged

chains, and greatly reduce the number of threefold-bonded defects which is believed to be contained in pure liquid Te and is responsible for the metallic conduction. This explains the decrease in the electrical conductivity with increasing alkali elements in experiment. In the case of equiatomic mixture  $\text{K}_{0.5}\text{Te}_{0.5}$ , the measured structure shows a virtually complete pairing of Te atoms.

Recently, Kawakita *et al.*<sup>6,7</sup> reported the results of their experiments on the electrical conductivity, the density, the EXAFS and the neutron scattering for liquid K- and Rb-Te mixtures. The separation of the first peak of the pair distribution function  $g(r)$  from the rest of neighbors becomes clear when alkali elements are added, and the Te-Te coordination number decreases with increasing alkali concentration. The position of the first peak of  $g(r)$  is nearly independent of alkali concentration. These results are consistent with those of Fortner *et al.*<sup>5</sup>

These experiments naturally indicate that the charge transfer from alkali elements to Te occurs in the liquid mixture. However, the spatial distribution of the transferred charge in the Te chains and the microscopic atomic configuration of the liquid alkali-Te mixtures have not yet been investigated theoretically. In this paper, we present the results of our *ab initio* molecular-dynamics (MD) simulations for investigating the structural and electronic properties of liquid Rb-Te mixtures. The purposes of our study are (i) to examine the atomic structure, especially the dependence of the Te chain structure on the concentration of Rb, (ii) to estimate the amount of the charge transfer from Rb to Te, and (iii) to investigate the spatial distribution of transferred (excess) charge in the Te chains. In Sec. II, the method of the first-principles MD simulation used here is briefly described. The results of our simulation and discussions are given in Secs. III and IV, respectively. Finally our conclusion is given in Sec. V.

## II. METHOD OF CALCULATION

Our calculations are performed within the framework of the density functional theory, in which the generalized gradient approximation proposed by Perdew and Wang<sup>8</sup> (PW91) is used for the exchange-correlation energy. The electronic wavefunctions are expanded in the plane-wave (PW) basis set. The energy functional is minimized using an iterative scheme based on the preconditioned conjugate-gradient method.<sup>9–11</sup> For the interaction between the valence and core electrons, we used the ultrasoft pseudopotential proposed by Vanderbilt.<sup>12</sup> The scheme for the pseudization of the wavefunctions and that for the calculation of the augmentation functions are described in Ref. 13. The valence-electron configurations of atoms Rb( $4p^6 4d^0 5s^1$ ) and Te( $5s^2 5p^4 5d^0$ ) are used in generating pseudopotentials.

The cubic supercell contains 80 atoms and the periodic boundary conditions are imposed. The simulations are carried out at three Rb concentrations;  $\text{Rb}_x\text{Te}_{1-x}$  with  $x=0.0, 0.2, \text{ and } 0.5$ . The temperatures and densities are (750 K,  $0.0272 \text{ \AA}^{-3}$ ), (710 K,  $0.0196 \text{ \AA}^{-3}$ ) and (710 K,  $0.0177 \text{ \AA}^{-3}$ ) for  $x=0.0, 0.2, \text{ and } 0.5$ , respectively. Using the Nosé-Hoover thermostat technique,<sup>14,15</sup> the equations of motion are solved via the velocity Verlet algorithm with a time step  $\Delta t=3.6 \times 10^{-15}$  s. The  $\Gamma$  point is used for the Brillouin zone sampling, and the PW cutoff energies for the wave functions and the charge density are 8.5 and 55 Ry, respectively, which are chosen so as to give a good convergence of the total energy. The initial charge density at each MD step is estimated by extrapolating the charge densities at the previous steps,<sup>11</sup> and the initial wave functions are estimated from the wave functions at the previous steps by means of a subspace diagonalization.<sup>10</sup> The quantities of interest are obtained by averaging over about 5 ps after the initial equilibration taking about 2 ps.

## III. RESULTS

### A. Atomic structure

To compare the calculated atomic structure with the experimental data, we show in Fig. 1 the structure factors  $S(k)$  for three Rb concentrations,  $x=0.0, 0.2, \text{ and } 0.5$ . The calculated  $S(k)$  shown by the solid line is obtained from the partial structure factors with the neutron scattering lengths ( $b_{\text{Te}}=5.43$  fm and  $b_{\text{Rb}}=7.08$  fm). The dashed and dotted lines show the results of neutron diffraction measurements by Kawakita *et al.*<sup>6,7</sup> and Takeda *et al.*,<sup>1</sup> respectively. We are unaware of any experimental measurement for  $x=0.5$ . We can see from Fig. 1 that the overall profile of the measured  $S(k)$  of the pure liquid Te is reproduced fairly well by our simulation and that the calculated  $S(k)$  of liquid  $\text{Rb}_{0.2}\text{Te}_{0.8}$  is in good agreement with the experiments. It should be noted that the position of the first peak shifts slightly to small  $k$  side when the Rb atoms are added.

The Ashcroft-Langreth partial structure factors<sup>16</sup> are defined as

$$S_{\alpha\beta}(k) = (N_\alpha N_\beta)^{-1/2} \left[ \left\langle \sum_{i=1}^{N_\alpha} \sum_{j=1}^{N_\beta} \exp\{-ik \cdot (\mathbf{r}_{ai} - \mathbf{r}_{\beta j})\} \right\rangle - (N_\alpha N_\beta)^{1/2} \delta_{k,0} \right], \quad (1)$$

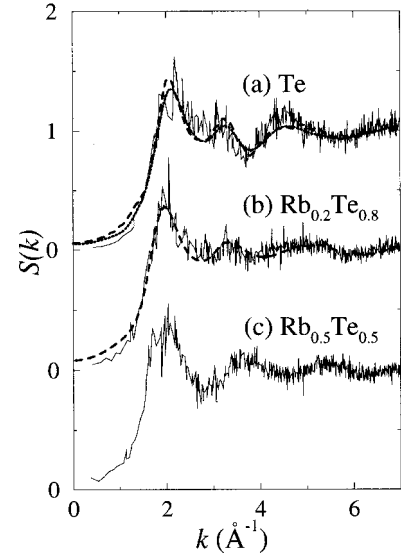


FIG. 1. The structure factors  $S(k)$  of liquid  $\text{Rb}_x\text{Te}_{1-x}$  for three Rb concentrations  $x =$  (a) 0.0, (b) 0.2, and (c) 0.5. The calculated  $S(k)$  shown by the solid line is obtained from the partial structure factors with the neutron scattering lengths. The dashed and dotted lines show the results of neutron diffraction measurements by Kawakita *et al.* (Ref. 7) and Takeda *et al.* (Ref. 1), respectively.

where  $N_\alpha$  is the total number of  $\alpha$ -type atoms, and  $\mathbf{r}_{ai}$  is the position of  $i$ th  $\alpha$ -type atom. The  $S_{\alpha\beta}(k)$  for  $x=0.2$  and  $0.5$  are shown in Figs. 2 and 3, respectively. There is a peak at  $k=1.1 \text{ \AA}^{-1}$  of the  $S_{\text{TeTe}}(k)$ , and this peak becomes higher with increasing Rb concentration. In the  $S_{\text{RbRb}}(k)$ , the corresponding peak is recognized, though its height is unchanged even when the Rb concentration is increased. Since the negative dip at  $k=1.1 \text{ \AA}^{-1}$  of the  $S_{\text{RbTe}}(k)$  cancels the peaks of the  $S_{\text{TeTe}}(k)$  and  $S_{\text{RbRb}}(k)$ , the total  $S(k)$  for  $x=0.2$  and  $0.5$  has no peak around  $k=1.1 \text{ \AA}^{-1}$  as shown in Figs. 1(b) and 1(c). The first peak of the total  $S(k)$  is originated from the peaks at about  $k=2 \text{ \AA}^{-1}$  of the  $S_{\text{TeTe}}(k)$  and  $S_{\text{RbTe}}(k)$ . The

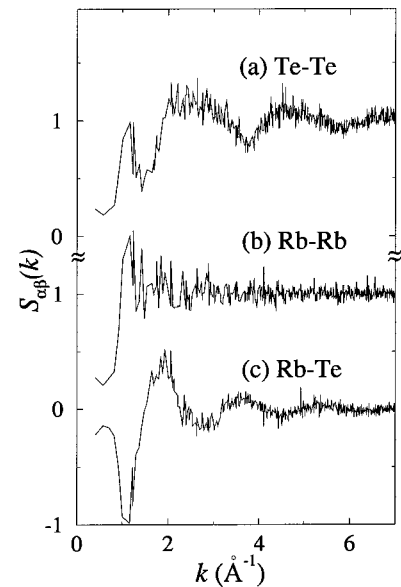


FIG. 2. The Ashcroft-Langreth partial structure factors  $S_{\alpha\beta}(k)$  of liquid  $\text{Rb}_{0.2}\text{Te}_{0.8}$ .

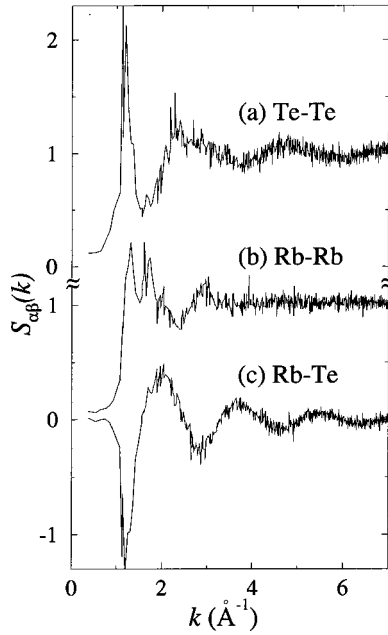


FIG. 3. The Ashcroft-Langreth partial structure factors  $S_{\alpha\beta}(k)$  of liquid  $\text{Rb}_{0.5}\text{Te}_{0.5}$ .

shift of the first-peak position observed in the total  $S(k)$  is caused by the fact that the corresponding peak of the  $S_{\text{RbTe}}(k)$  is in the smaller  $k$  region compared with that of the  $S_{\text{TeTe}}(k)$ .

The Bhatia-Thornton concentration-concentration structure factor<sup>17</sup> is defined as

$$S_{\text{CC}}(k) = c_{\text{Te}}c_{\text{Rb}}\{c_{\text{Rb}}S_{\text{TeTe}}(k) + c_{\text{Te}}S_{\text{RbRb}}(k) - 2(c_{\text{Te}}c_{\text{Rb}})^{1/2}S_{\text{RbTe}}(k)\}, \quad (2)$$

where  $c_{\text{Te}}, c_{\text{Rb}}$  are the concentrations of Te and Rb atoms, respectively. In Fig. 4, the  $S_{\text{CC}}(k)$  for  $x=0.2$  and  $0.5$  are presented. The profiles of the  $S_{\text{CC}}(k)$  are much different

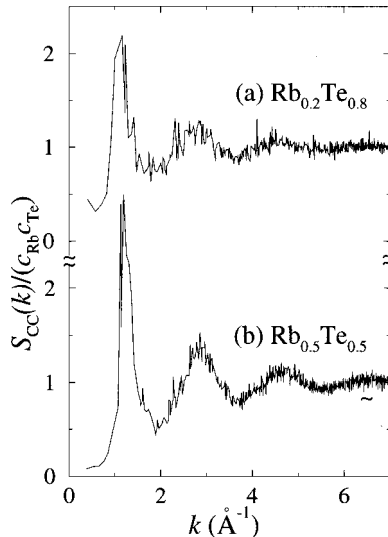


FIG. 4. The Bhatia-Thornton concentration-concentration structure factors  $S_{\text{CC}}(k)/(c_{\text{Rb}}c_{\text{Te}})$  of liquid  $\text{Rb}_x\text{Te}_{1-x}$  for two Rb concentrations  $x =$  (a) 0.2 and (b) 0.5, where the  $c_{\text{Rb}}$  and  $c_{\text{Te}}$  are the concentrations of Rb and Te, respectively.

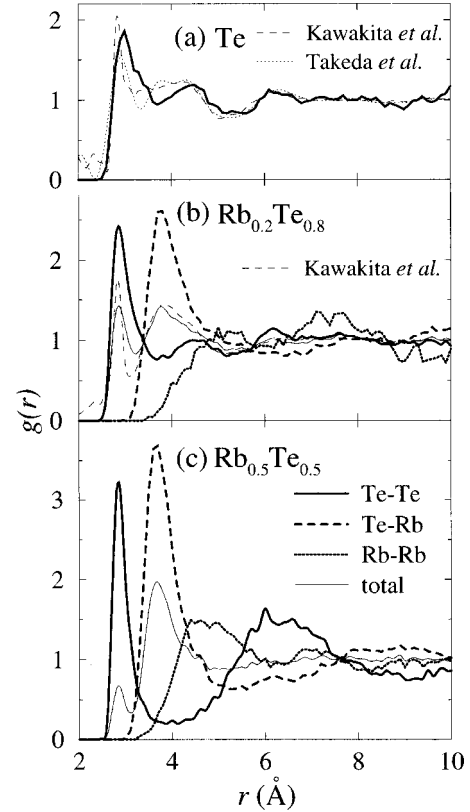


FIG. 5. The pair distribution functions  $g(r)$  of liquid  $\text{Rb}_x\text{Te}_{1-x}$  for three Rb concentrations  $x =$  (a) 0.0, (b) 0.2, and (c) 0.5. The bold-solid, bold-dashed, and bold-dotted lines show the calculated results for the Te-Te, Te-Rb, and Rb-Rb partial pair distribution functions, respectively. The thin solid lines in (b) and (c) show the total  $g(r)$  calculated with the neutron scattering lengths. The thin-dashed and thin-dotted lines show the results of neutron diffraction measurements by Kawakita *et al.* (Refs. 6 and 7) and Takeda *et al.* (Ref. 1), respectively.

from those of the  $S(k)$ . The  $S_{\text{CC}}(k)$  has a large peak at about  $k=1.1 \text{ \AA}^{-1}$ , which becomes higher with increasing  $x$ . This peak corresponds to a concentration-concentration correlation with length scale of about  $6 \text{ \AA}$ , which will arise from some charge ordering in the liquid mixtures.

Figure 5 shows the pair distribution functions  $g(r)$ . The bold-solid, bold-dashed and bold-dotted lines show the Te-Te, Te-Rb, and Rb-Rb partial pair distribution functions, respectively. In Figs. 5(b) and 5(c), the total pair distribution functions calculated from the partial pair distribution functions with the neutron scattering lengths are shown by the thin solid lines to compare them with experiments.<sup>6,7,1</sup>

From Fig. 5(a), we can see that there is a fair agreement between the experimental and calculated  $g(r)$ 's for the liquid Te in the sense that there is no well-defined first coordination shell in both  $g(r)$ 's. On the other hand, as shown in Fig. 5(b), the calculated total  $g(r)$  is in reasonable agreement with the experiments for  $\text{Rb}_{0.2}\text{Te}_{0.8}$ ; the first- and second-peak positions as well as the position of the first minimum of the calculated  $g(r)$  are in good agreement with those of the experimental  $g(r)$ .

From Figs. 5(b) and 5(c), the first and second peaks of the total  $g(r)$  are attributed to the  $g_{\text{TeTe}}(r)$  and  $g_{\text{TeRb}}(r)$ , respec-

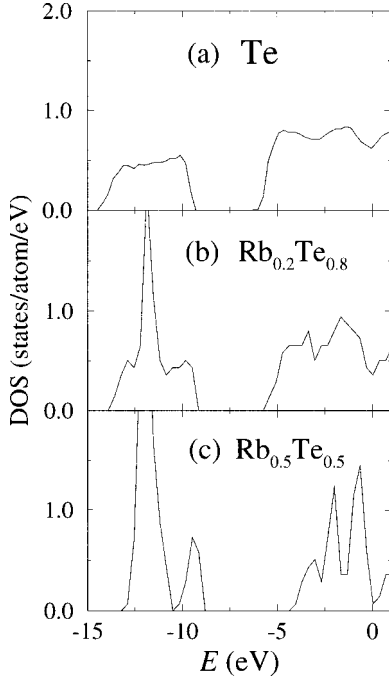


FIG. 6. The electronic density of states (DOS) of liquid  $\text{Rb}_x\text{Te}_{1-x}$  for three Rb concentrations  $x =$  (a) 0.0, (b) 0.2, and (c) 0.5. The origin of the energy is taken to be the Fermi level ( $E_F = 0$ ).

tively. The peaks of these two partial  $g(r)$ 's become higher with increasing Rb concentration. The first minimum of the  $g_{\text{TeTe}}(r)$  becomes deeper when the Rb concentration is increased. As for the  $g_{\text{RbRb}}(r)$ , it has broad distribution for both concentrations  $x = 0.2$  and 0.5, though a plateau around  $4.5 \text{ \AA}$  is recognized at  $x = 0.5$ .

### B. Electronic density of states

Figure 6 shows the concentration dependence of the electronic density of states (DOS) in liquid Rb-Te mixtures, which is obtained from a time average of the distribution of the single-electron eigenvalues. The origin of the energy is taken to be the Fermi level ( $E_F = 0$ ). From Fig. 6(a), the DOS has large values around  $E_F$ , which means the metallic properties of pure liquid Te is reproduced. As shown in Figs. 6(b) and 6(c), a dip at  $E_F$  in the DOS arises from the presence of Rb atoms, and the dip becomes deeper with increasing Rb concentration, which is consistent with the observed concentration dependence of the electrical conductivity.<sup>7</sup>

The partial DOS of the liquid  $\text{Rb}_x\text{Te}_{1-x}$  for two concentrations  $x = 0.2$  and 0.5 are shown in Fig. 7, where the dashed and solid lines show the  $s$  and  $p$  components, respectively. The partial DOS was obtained by projecting the wavefunctions on the spherical harmonics within a sphere of radius  $S = 1.1 \text{ \AA}$  centered at each atom. The Te  $5s$  states are located between  $-13$  and  $-8 \text{ eV}$ , and the Te  $5p$  states are located above  $-5 \text{ eV}$ . At  $x = 0.5$ , there are several sharp peaks in the partial DOS for Te; two peaks in the  $5s$  states and three peaks in the  $5p$  states below  $E_F$  correspond to the energy levels of  $\text{Te}_2^{2-}$  dimer. The large peak at  $-12 \text{ eV}$  observed in the total DOS originates from the Rb  $4p$  states.

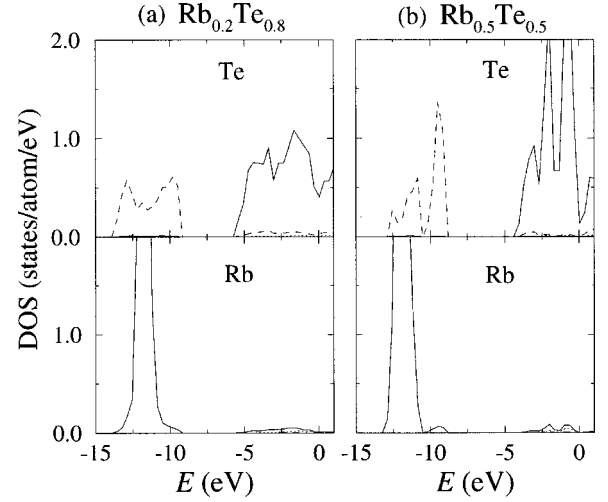


FIG. 7. The partial electronic density of states (DOS) of  $\text{Rb}_x\text{Te}_{1-x}$  for two Rb concentrations  $x =$  (a) 0.2 and (b) 0.5. The dashed and solid lines show the  $s$  and  $p$  components, respectively.

The partial DOS for Rb has very small values above  $-5 \text{ eV}$  for both concentrations, and these values are almost unchanged even if larger radii, e.g.,  $S = 2 \text{ \AA}$ , are used. This behavior is quite consistent with the results of calculation for the electron-ion correlation function  $g_{ei}(r)$ . When the  $g_{ei}(r)$  is decomposed into its angular momentum components around each Rb atom, we observe that main contribution to the  $g_{ei}(r)$  is the  $p$  component, and the contribution of the  $s$  component is very small up to distances where the neighboring Te atoms exist. From these facts, we conclude that there exists almost no occupied state originating from the  $5s$  states around Rb atoms, and that nearly complete charge transfer from Rb to Te occurs.

### C. Spatial distribution of excess charge

In order to investigate the spatial distribution of transferred charge in the Te chains, we prepare three electronic charge density distributions; (1) the charge density distribution  $\rho(\mathbf{r})$  for the liquid Rb-Te mixtures obtained by the *ab initio* MD simulation, (2) the charge density distribution  $\rho_{\text{Te}}(\mathbf{r})$  obtained from a self-consistent electronic states calculation for a system containing only Te atoms which is obtained from the atomic configuration of the Rb-Te mixture by removing Rb atoms only, and (3) the charge density distribution  $\rho_{\text{Rb}}^{4p}(\mathbf{r})$  calculated as

$$\rho_{\text{Rb}}^{4p}(\mathbf{r}) = \sum_i \rho_{\text{Rb atom}}^{4p}(\mathbf{r} - \mathbf{r}_i), \quad (3)$$

where  $\rho_{\text{Rb atom}}^{4p}(\mathbf{r})$  is the  $4p$  electron density distribution around a Rb atom obtained by the electronic states calculation for a  $\text{Rb}^+$  ion, and  $\mathbf{r}_i$  is the position of  $i$ th Rb atom in the Rb-Te mixture. Using these three charge densities, we can define the excess charge in the Te chains transferred from Rb atoms as

$$\Delta\rho(\mathbf{r}) = \rho(\mathbf{r}) - \rho_{\text{Te}}(\mathbf{r}) - \rho_{\text{Rb}}^{4p}(\mathbf{r}). \quad (4)$$

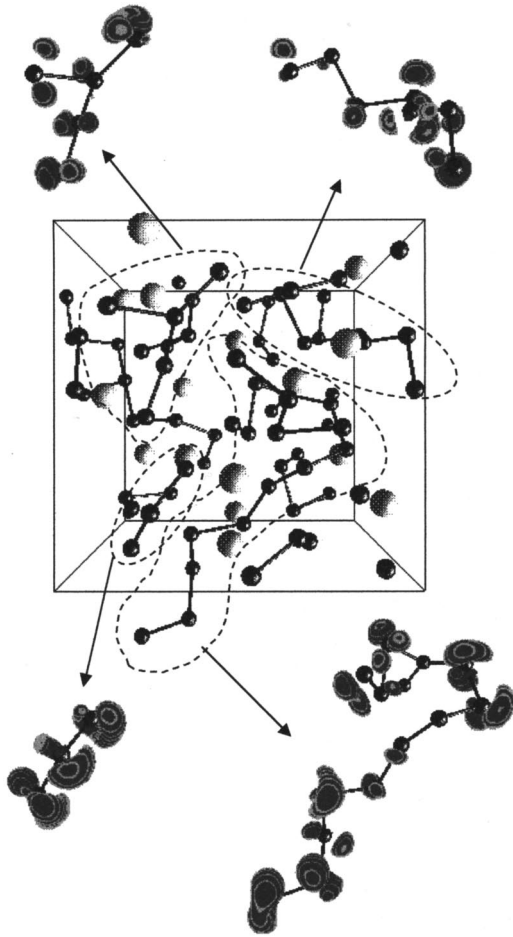


FIG. 8. Atomic configuration and spatial distribution of the excess charge  $\Delta\rho(\mathbf{r})$  for  $\text{Rb}_{0.2}\text{Te}_{0.8}$ . The frame shows the MD cell, and the black and gray balls show the Te and Rb atoms, respectively. Two Te atoms, whose distance apart is smaller than  $3.1 \text{ \AA}$ , are connected by the bond. The spatial distributions of the  $\Delta\rho(\mathbf{r})$  around some selected Te chains are shown outside the MD cell; the contour surfaces are drawn for the charge density of  $0.0025 \text{ a.u.}$

The spatial distributions of the  $\Delta\rho(\mathbf{r})$  as well as the atomic configurations in the MD cell for two Rb concentrations  $x=0.2$  and  $0.5$  are displayed in Figs. 8 and 9, respectively. The frame in each figure shows the MD cell, and the black and gray balls show the Te and Rb atoms, respectively. Two Te atoms, whose distance apart is smaller than  $3.1 \text{ \AA}$ , are connected by the bond. The spatial distributions of the  $\Delta\rho(\mathbf{r})$  around some selected Te chains are shown outside the MD cell; the contour surfaces are drawn for the charge density of  $0.0025 \text{ a.u.}$

It is seen from Fig. 8 that, for  $x=0.2$ , the Te atoms have a chain structure in which relatively long chains are included, and that the  $\Delta\rho(\mathbf{r})$  distributes nonuniformly in the Te chains. On the other hand, as shown in Fig. 9, for  $x=0.5$ , more than half of the Te atoms form dimers and the rest are present in short chains. The distributions of the  $\Delta\rho(\mathbf{r})$  around the dimers are similar to each other, i.e. a “dumbbell-shaped” distribution as expected by Fortner *et al.*<sup>5</sup>

#### IV. DISCUSSION

Fortner *et al.* suggested, from their neutron-diffraction<sup>5</sup> and Raman-scattering<sup>18</sup> measurements for the liquid K-Te

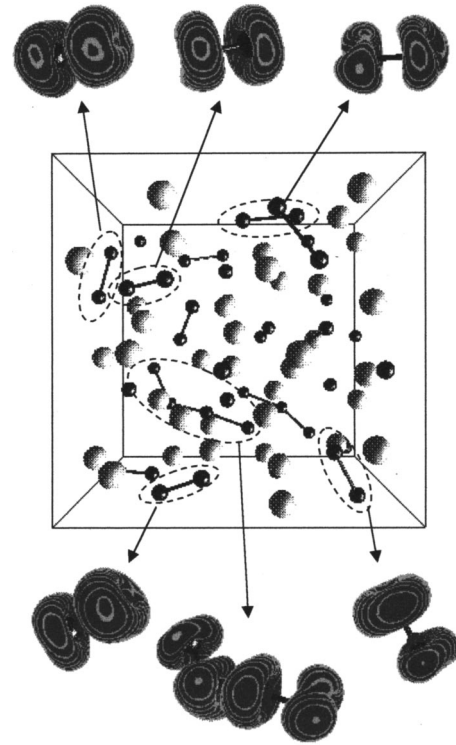


FIG. 9. Atomic configuration and spatial distribution of the excess charge  $\Delta\rho(\mathbf{r})$  for  $\text{Rb}_{0.5}\text{Te}_{0.5}$ . Refer to the caption of Fig. 8.

mixture, that a transition to a true twofold-coordinated covalent bonding of Te in the liquid occurs on addition of K, while pure liquid Te contains some other type of bonding. As shown in Fig. 5, it is found from our MD simulations that the first peak of the  $g_{\text{TeTe}}(r)$  becomes higher, and its first minimum becomes deeper when the Rb atoms are added into the liquid Te. These results show a clear evidence for a well-defined first coordination shell for the Te-Te pairs and are consistent with the conclusion of Fortner *et al.*<sup>5</sup> To see the calculated chain structure of Te in the Rb-Te mixtures clearly, we obtain the Te-Te coordination number ( $n$ ) distribution function  $P(n)$ , which is calculated simply by counting the number of Te atoms inside a sphere of radius  $R$  centered at each Te atom. Figure 10 displays the  $P(n)$ 's for three Rb concentrations  $x=0.0, 0.2$ , and  $0.5$ , which are shown by the circles, squares and diamonds, respectively. We use  $R=3.1 \text{ \AA}$ . Although the  $P(n)$  depends somewhat on the value of  $R$ , the qualitative features of  $P(n)$  never change unless unreasonable value of  $R$  is used. The  $P(n)$  for the pure liquid Te has the largest value at  $n=2$ , and the value of  $P(3)$  is slightly smaller than that of  $P(2)$ . For  $x=0.2$ , the  $P(n)$  for  $n \geq 3$  decrease, and the  $P(n)$  for  $n \leq 2$  increase. This means that the interactions between Te chains are suppressed by the presence of alkali elements and that the twofold-coordinated chain structure is relatively stabilized. For  $x=0.5$ , the  $P(n)$  has a large peak at  $n=1$ , which results from the presence of a large number of  $\text{Te}_2^{2-}$  dimers. It is interesting to note that the  $P(2)$  has a finite value even for  $x=0.5$ , which means that there remain the Te chains consisting of more than two atoms, as already shown in Fig. 9, despite of the almost complete charge transfer from Rb to Te.

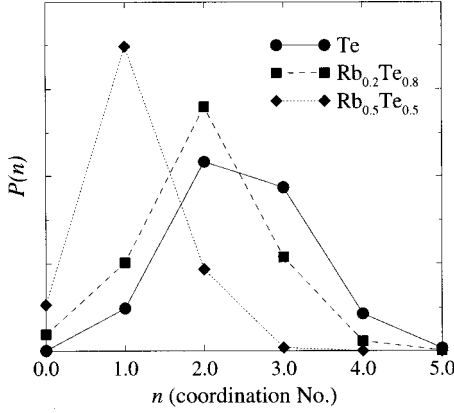


FIG. 10. The Te-Te coordination number ( $n$ ) distribution function  $P(n)$  of liquid  $\text{Rb}_x\text{Te}_{1-x}$  for three Rb concentrations  $x=0.0$ , 0.2, and 0.5, which are shown by the circles, squares, and diamonds, respectively.

As stated in Sec. III C, the transferred excess charge  $\Delta\rho(\mathbf{r})$  for  $x=0.5$  has a “dumbbell-shaped” distribution around a pair of Te atoms. This feature is quite understandable for  $\text{Te}_2^{2-}$  dimers. As for  $x=0.2$ , the nonuniform distribution of  $\Delta\rho(\mathbf{r})$  in the Te chains as shown in Fig. 8 is explained below by the total excess charge  $\Delta N_i$  for  $i$ th Te atom. It is defined as

$$\Delta N_i = \int_{|r-r_i| \leq D} d\mathbf{r} \Delta\rho(\mathbf{r}), \quad (5)$$

where  $\mathbf{r}_i$  is the position of the  $i$ th Te atom and  $D$  the radius of a sphere centered at each Te atom. We investigate the following relations: (1) the relation between the  $\Delta N_i$  and the Te coordination number  $n_i$  for the  $i$ th Te atom, and (2) the relation between the  $\Delta N_i$  and the Rb-Te distance  $R_i^{\text{Rb-Te}}$ , which is defined by the distance from the  $i$ th Te atom to its nearest Rb atom. Figures 11(a) and 11(b) show the  $\Delta N_i$  vs  $n_i$  and the  $\Delta N_i$  vs  $R_i^{\text{Rb-Te}}$  relations, respectively, calculated for  $x=0.2$  using  $D=1.1 \text{ \AA}$ . It should be noted again that, although the values of  $\Delta N_i$  depend quantitatively on the choice of the value of the radius  $D$ , the qualitative features of the above two relations are unchanged. It is found that the  $\Delta N_i$  depends weakly on  $n_i$ ; the  $\Delta N_i$  for  $n_i=2$  distributes over slightly larger values than that for  $n_i=3$ . On the other hand, the  $\Delta N_i$  has strong correlation with  $R_i^{\text{Rb-Te}}$ ; the  $\Delta N_i$  increases with decreasing  $R_i^{\text{Rb-Te}}$ . Thus, in the case of  $x=0.2$ , the distribution of the excess charge in the Te chains is very sensitive to the positions of alkali atoms.

## V. CONCLUSIONS

The structural and electronic properties of liquid  $\text{Rb}_x\text{Te}_{1-x}$  mixtures with  $x=0.0$ , 0.2 and 0.5 are studied by an *ab initio* molecular-dynamics (MD) simulation. From the calculated concentration dependence of the electronic den-

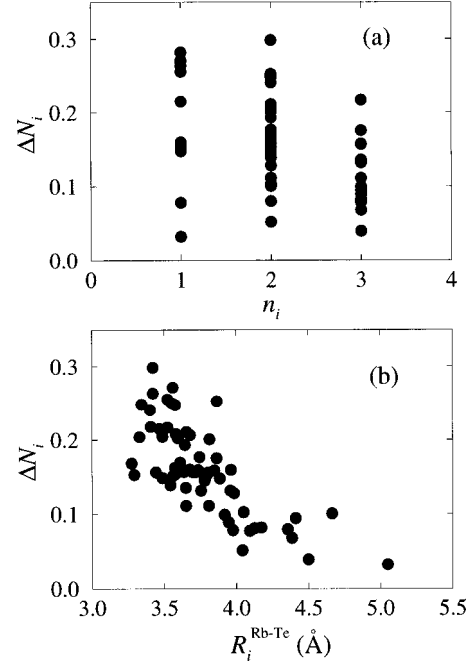


FIG. 11. (a) The relation between the Te coordination number  $n_i$  and the total excess charge  $\Delta N_i$  for  $i$ th Te atom, and (b) the relation between the Rb-Te distance  $R_i^{\text{Rb-Te}}$  and the  $\Delta N_i$  for  $\text{Rb}_{0.2}\text{Te}_{0.8}$ .

sity of states (DOS), we conclude that the metal-semiconductor transition in liquid Rb-Te mixtures has been successfully reproduced by our *ab initio* MD simulations. This metal-semiconductor transition is closely related to the structural change in the Te chain. It is confirmed that, for  $x=0.2$ , the interaction between two Te chains are suppressed by the presence of alkali elements, and as a result the twofold-coordinated chain becomes more stable. For  $x=0.5$ , more than half of Te atoms form  $\text{Te}_2^{2-}$  dimers, and the rest form the short Te chains consisting of more than two atoms. It is also concluded from the partial DOS that almost complete charge transfer from Rb to Te occurs in the mixtures. At the low Rb concentration, the excess charge transferred from Rb atoms distributes nonuniformly in Te chains, depending very sensitively on the positions of neighboring Rb atoms. At the equiatomic mixture, the excess charge has a “dumbbell-shaped” distribution around a pair of Te atoms as expected by Fortner *et al.*<sup>5</sup>

## ACKNOWLEDGMENTS

We would like to thank Dr. Y. Kawakita, Professor M. Yao, and Professor S. Takeda for providing us with their experimental data. This work was supported by a Grant-in-Aid for Scientific Research (No. 07236102, No. 09740287, and No. 10640370) from The Ministry of Education, Science, Sports and Culture, Japan. We also wish to thank the Supercomputer Center, Institute for Solid State Physics, University of Tokyo for the use of the FACOM VPP500.

- <sup>1</sup>S. Takeda, S. Tamaki, and Y. Waseda, *J. Phys. Soc. Jpn.* **53**, 3830 (1984).
- <sup>2</sup>A. Munelle, R. Bellissent, and A. M. Frank, *Physica B* **156&157**, 174 (1989).
- <sup>3</sup>T. Tsuzuki, M. Yao, and H. Endo, *J. Phys. Soc. Jpn.* **64**, 485 (1995).
- <sup>4</sup>A. Petric, A. D. Pelton, and M.-L. Saboungi, *J. Chem. Phys.* **89**, 5070 (1988).
- <sup>5</sup>J. Fortner, M.-L. Saboungi, and J. E. Enderby, *Phys. Rev. Lett.* **69**, 1415 (1992).
- <sup>6</sup>Y. Kawakita, M. Yao, H. Endo, and J. Dong, *J. Non-Cryst. Solids* **205-207**, 447 (1996).
- <sup>7</sup>Y. Kawakita, M. Yao, and H. Endo, *J. Phys. Soc. Jpn.* **66**, 1339 (1997).
- <sup>8</sup>J. P. Perdew, in *Electronic Structure of Solids '91*, edited by P. Ziesche and H. Eschrig (Akademie Verlag, Berlin, 1991); J. P. Perdew, J. A. Chevary, S. H. Vosko, K. A. Jackson, M. R. Pederson, D. J. Singh, and C. Fiolhais, *Phys. Rev. B* **46**, 6671 (1992).
- <sup>9</sup>F. Shimojo, Y. Zempo, K. Hoshino, and M. Watabe, *Phys. Rev. B* **52**, 9320 (1995).
- <sup>10</sup>T. A. Arias, M. C. Payne, and J. D. Joannopoulos, *Phys. Rev. B* **45**, 1538 (1992).
- <sup>11</sup>G. Kresse and J. Hafner, *Phys. Rev. B* **49**, 14 251 (1994).
- <sup>12</sup>D. Vanderbilt, *Phys. Rev. B* **41**, 7892 (1990).
- <sup>13</sup>G. Kresse and J. Hafner, *J. Phys.: Condens. Matter* **6**, 8245 (1994).
- <sup>14</sup>S. Nosé, *Mol. Phys.* **52**, 255 (1984).
- <sup>15</sup>W. G. Hoover, *Phys. Rev. A* **31**, 1695 (1985).
- <sup>16</sup>N. W. Ashcroft and D. C. Langreth, *Phys. Rev.* **159**, 500 (1967).
- <sup>17</sup>A. B. Bhatia and D. E. Thornton, *Phys. Rev. B* **2**, 3004 (1970).
- <sup>18</sup>J. Fortner and M.-L. Saboungi, *Europhys. Lett.* **22**, 359 (1993).